Isı Bilimi ve Tekniği Dergisi, 29, 1, 67-78, 2009
J. of Thermal Science and Technology

ISSN 1300-3615

FORCED CONVECTION HEAT TRANSFER IN ECCENTRIC CURVED ANNULAR SQUARE DUCTS

Haydar KÜÇÜK* **ve Habip ASAN****
*Karadeniz Technical University, Department of Naval Architecture and Marine Engineering,
61530, Çamburnu, Trabzon, hkucuk@ktu.edu.tr
**Karadeniz Technical University, Department of Mechanical Engineering,
61080 Trabzon, asan@ktu.edu.tr

(Geliş Tarihi: 11. 11. 2008, Kabul Tarihi: 23. 01. 2009)

Abstract: Hydrodynamically and thermally fully developed, steady, incompressible laminar flow with constant physical properties in eccentric curved annular square duct was investigated numerically. Inner and outer walls were assumed to be isothermal, but at different temperatures. For the Cartesian coordinate system, the continuity, momentum and energy equations included the curvature ratio were discretized by using control volume finite difference method and the dependent variables in the governing equations were solved by ADI method uses the TDMA. The Stone's method was employed to solve the pressure-correction equation instead of ADI method. The upwind scheme and the central difference scheme were employed to represent the convection and diffusion terms, respectively. Solutions were obtained for air (Pr=0.7). Secondary flow streamlines, velocity and temperature fields, velocity profiles, the friction coefficients and average and local Nusselt numbers were presented depending on Dean number and annulus dimension ratio (a/b). It was observed that secondary flow resulting from centrifugal force highly affects the velocity and temperature fields. It has seen that curvature, annulus dimension ratio and core position affect heat transfer and friction factor. With the increasing annulus dimension ratio, it has been shown that the convective heat transfer is remarkably enhanced at both the inner and the outer walls.
Keywords: Laminar flow, Heat transfer, Curved annular duct, Eccentric, Constant wall temperature.

KAÇIK MERKEZLİ HALKA KESİTLİ EĞRİSEL KARE KANALLARDA ZORLANMIŞ TAŞINIMLA ISI TRANSFERİ

Özet: Kaçık merkezli halka kesite sahip eğrisel kare kanallarda tam gelişmiş, sürekli, sıkıştırılamaz, sabit fiziksel özeliklere sahip laminer akış sayısal olarak incelenmiştir. İç ve dış duvarlarda birbirinden farklı olmak koşuluyla sabit yüzey sıcaklığı öngörülmüştür. Eğrilik oranının da içinde bulunduğu kartezyen koordinatlarda ifade edilmiş süreklilik, momentum ve enerji denklemleri sonlu fark kontrol hacim yöntemiyle ayrıklaştırılmış ve denklemlerdeki bağımlı değişkenler üç köşegenli bant matris algoritmasını kullanan ADI metoduyla çözülmüştür. Basınç-doğrultman denklemini çözmek için ADI metodu yerine Stone metodu kullanılmıştır. Taşınım ve yayınım terimleri sırasıyla yukarı fark ve merkezi fark yöntemiyle ayrıklaştırılmıştır. Çözümler hava için elde edilmiştir (Pr=0.7). İkincil akış akım çizgileri, hız ve sıcaklık alanları, hız profilleri, sürtünme faktörü ve ortalama ve yerel Nusselt sayıları Dean sayısı ve halka kesit boyut oranına (a/b) bağlı olarak gösterilmiştir. Merkezkaç kuvvetlerden kaynaklanan ikincil akışların hız ve sıcaklık alanlarını önemli ölçüde etkilediği gözlenmiştir. Eğriliğin, halka kesit boyut oranının ve içteki elemanın konumunun ısı transferi ve sürtünme faktörünü etkilediği görülmüştür. Boyut oranının artışıyla, ısı transferinin iç ve dış duvarlarda önemli düzeyde arttığı belirlenmiştir.
Anahtar kelimeler: Laminer akış, Isı transferi, Eğrisel halka kesitli kanal, Kaçık merkezli, Sabit yüzey sıcaklığı.

NOMENCLATURE

a	Width or height of the outer wall [m]
A	Cross-sectional area of the annular duct [m^2]
b	Width or height of the inner wall [m]
cA	Case A
cB	Case B
cw	Core wall
dP/dz	Axial pressure gradient [Pa/m]
dP^+/dz^+	Dimensionless axial pressure gradient
dT/dz	Axial temperature gradient [K/m]
dT^+/dz^+	Dimensionless axial temperature gradient
De	Dean number, Eq. (19)
D_h	Hydraulic diameter [m]
dw	Duct wall
f	Friction factor
l	Circumferential length of channel wall
l'	Circumferential length of core wall
Nu	Nusselt number
P	Pressure [Pa]
P^+	Dimensionless pressure, Eq. (6)

Pr	Prandtl number, Eq. (6)
Re	Reynolds number, Eq. (18)
r^+	Dimensionless radius of curvature, Eq. (6)
R	Radius of curvature of a curved channel [m]
S	Source term
T	Temperature [K]
T^+	Dimensionless temperature, Eq. (6)
u, v, w	Velocity components in x-, y- and z-directions [m/s]
u^+, v^+, w^+	Dimensionless velocity components in x-, y- and z-directions, Eq. (6)
x, y, z	Cartesian coordinates [m]
x^+, y^+, z^+	Dimensionless coordinates in x-, y- and z-directions, Eq. (6)

Greek symbols

α	Thermal diffusivity [m^2/s]
Γ	Diffusion coefficient
μ	Dynamic viscosity [kg/s m]
ν	Kinematic viscosity [m^2/s]
ρ	Density [kg/m^3]
ϕ	Dependent variable

Subscripts

c	Value for a curved channel, cold
h	Hot
i	Inner
L	Local
m	Mean value
o	Outer

INTRODUCTION

Curved annular ducts have several applications in engineering such as double-pipe heat exchangers, air conditioning systems, cooling systems, gas turbines, chemical mixing and drying machinery. The secondary flows passages originate principally from the interaction between the centrifugal force, the pressure gradient, and the viscous forces. The flow in a curved annulus is significantly different from that in a curved pipe because of the presence of an inner pipe around which an additional inner wall boundary layer has to be established (Choi and Park, 1992). Kucuk and Asan (2009) numerically investigated fully developed laminar flow in a concentric curved annular duct under constant wall temperature boundary condition. They determined that viscous forces become more effective upon centrifugal forces while the annulus dimension ratio decreases. However, they found out that when the Dean number increases the centrifugal forces are more dominant than viscous forces. Also, they showed that the secondary flows resulting from centrifugal forces affect the distribution of the velocity and temperature fields. It is known that the Dean number and radius ratio highly affect the friction factor and the Nusselt number in curved circular annular ducts (Choi and Park, 1994; Petrakis and Karahalios, 1999). Petrakis and Karahalios (1997) presented numerical results for exponentially decaying flow in a gently curved annular pipe. They observed that the secondary flow exhibited two vortices rotating in opposite directions. They also found that the axial rigid core affected the flux through a cross section of the pipe. Garimella et al. (1988) experimentally studied forced convection heat transfer in coiled circular annular ducts. They concluded that coiling enhanced the heat transfer coefficients especially in the laminar region.

As a consequence of literature review, it was seen that no study on eccentric curved annular ducts with rectangular cross section has been performed. The purpose of this study is to present numerical results for both hydrodynamically and thermally fully developed laminar flow in eccentric curved annular duct with square cross-section. Constant wall temperature is assumed at walls.

ANALYSIS

The physical configuration and the coordinate system of the problem are shown in Fig. 1. All physical properties of the fluid are assumed constant. The governing equations for steady, hydrodynamically and thermally fully developed, incompressible laminar flow in the cross section in a curved duct can be written as (Dong and Ebadian, 1992; Gyves and Irvine, 2000; Gyves, 1997; Kucuk, 2003; Asan and Kucuk, 2007; Kucuk and Asan, 2009):

Continuity Equation

$$\frac{\partial u}{\partial x}+\frac{\partial v}{\partial y}+\frac{u}{R+x}=0 \tag{1}$$

Momentum Equations

$$u\frac{\partial u}{\partial x}+v\frac{\partial u}{\partial y}-\frac{w^2}{R+x}=-\frac{1}{\rho}\frac{\partial P}{\partial x}+\nu\left(\frac{\partial^2 u}{\partial x^2}+\frac{\partial^2 u}{\partial y^2}+\frac{1}{R+x}\frac{\partial u}{\partial x}-\frac{u}{(R+x)^2}\right) \tag{2}$$

$$u\frac{\partial v}{\partial x}+v\frac{\partial v}{\partial y}=-\frac{1}{\rho}\frac{\partial P}{\partial y}+\nu\left(\frac{\partial^2 v}{\partial x^2}+\frac{\partial^2 v}{\partial y^2}+\frac{1}{R+x}\frac{\partial v}{\partial x}\right) \tag{3}$$

$$u\frac{\partial w}{\partial x}+v\frac{\partial w}{\partial y}-\frac{uv}{R+x}=-\frac{R}{(R+x)\rho}\frac{\partial P}{\partial z}+\nu\left(\frac{\partial^2 w}{\partial x^2}+\frac{\partial^2 w}{\partial y^2}+\frac{1}{R+x}\frac{\partial w}{\partial x}-\frac{w}{(R+x)^2}\right) \tag{4}$$

Energy Equation

$$u\frac{\partial T}{\partial x}+v\frac{\partial T}{\partial y}+\frac{R}{(R+x)}w\frac{\partial T}{\partial z}= \alpha\left[\frac{\partial^2 T}{\partial x^2}+\frac{\partial^2 T}{\partial y^2}+\frac{1}{(R+x)}\frac{\partial T}{\partial x}\right] \quad (5)$$

It is assumed that the radius of curvature (R) is large compared with the channel dimensions (R+x≈R). The model neglects all terms of the order 1/R and $1/R^2$, with the exception of the centrifugal force term as given by Gyves (1997), Gyves and Irvine (2000); Kucuk (2003), Asan and Kucuk (2007), Kucuk and Asan (2009) and Gyves et al.(1999).

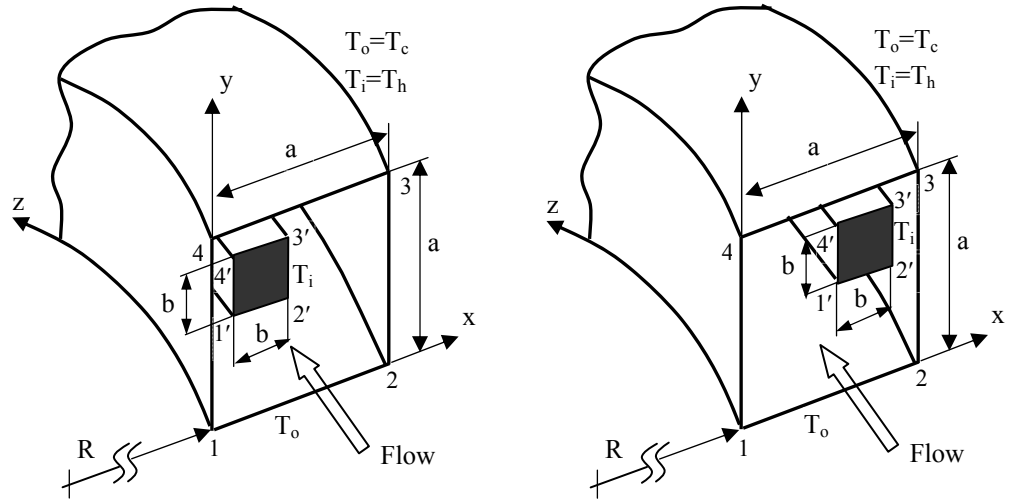

Figure 1. Problem geometry and coordinate system.

Equations (1-5) can be written as follows by using the above assumptions and by substituting the dimensionless variables given as below (Gyves and Irvine, 2000).

$$x^+=\frac{x}{D_h},\quad y^+=\frac{y}{D_h},\quad z^+=\frac{z}{D_h},\quad u^+=\frac{uD_h}{\nu}$$
$$v^+=\frac{vD_h}{\nu},\quad w^+=\frac{wD_h}{\nu},\quad P^+=\frac{P}{\rho\nu^2/D_h^2} \quad (6)$$
$$T^+=\frac{T-T_o}{T_i-T_o},\qquad \mathrm{Pr}=\frac{\nu}{\alpha},\qquad r^+=\frac{R}{D_h}$$

Continuity Equation

$$\frac{\partial u^+}{\partial x^+}+\frac{\partial v^+}{\partial y^+}=0 \quad (7)$$

Momentum Equations

$$u^+\frac{\partial u^+}{\partial x^+}+v^+\frac{\partial u^+}{\partial y^+}=-\frac{\partial P^+}{\partial x^+}+\frac{w^{+2}}{r^+}+\frac{\partial^2 u^+}{\partial x^{+2}}+\frac{\partial^2 u^+}{\partial y^{+2}} \quad (8)$$

$$u^+\frac{\partial v^+}{\partial x^+}+v^+\frac{\partial v^+}{\partial y^+}=-\frac{\partial P^+}{\partial y^+}+\frac{\partial^2 v^+}{\partial x^{+2}}+\frac{\partial^2 v^+}{\partial y^{+2}} \quad (9)$$

$$u^+\frac{\partial w^+}{\partial x^+}+v^+\frac{\partial w^+}{\partial y^+}=-\frac{\partial P^+}{\partial z^+}+\frac{\partial^2 w^+}{\partial x^{+2}}+\frac{\partial^2 w^+}{\partial y^{+2}} \quad (10)$$

Energy Equation

$$u^+\frac{\partial T^+}{\partial x^+}+v^+\frac{\partial T^+}{\partial y^+}+w^+\frac{\partial T^+}{\partial z^+}=\frac{1}{\mathrm{Pr}}\left(\frac{\partial^2 T^+}{\partial x^{+2}}+\frac{\partial^2 T^+}{\partial y^{+2}}\right) \quad (11)$$

The equations are subjected to the following boundary conditions at the channel and core walls:

$u^+=v^+=w^+=0$ at the channel and core walls (12)

$T^+=0$ at the channel wall (13)

$T^+=1$ at the core wall (14)

For hydrodynamically fully developed flow, the pressure gradient varies only in the cross-section of the curved channel. Therefore, the dimensionless axial pressure gradient remains constant at any axial position (Dong and Ebadian, 1991; Gyves and Irvine, 2000; Gyves et al. 1999; Dong and Ebadian, 1992). For thermally fully developed flow under axially and peripherally constant wall temperature boundary

condition the dimensionless axial temperature gradient is taken as zero at any axial position (Incropera and DeWitt, 1990; Çengel, 2003).

The equations (7-11) can be expressed in a generic form for a property, ϕ, as in the following:

$$\frac{\partial\left(u^{+}\phi\right)}{\partial x^{+}}+\frac{\partial\left(v^{+}\phi\right)}{\partial y^{+}}=\frac{\partial}{\partial x^{+}}\left(\Gamma_{\phi}\frac{\partial\phi}{\partial x^{+}}\right)+\frac{\partial}{\partial y^{+}}\left(\Gamma_{\phi}\frac{\partial\phi}{\partial y^{+}}\right)+S_{\phi} \tag{15}$$

For each conservation equation, the general dependent variable, ϕ, the diffusion coefficient, Γ_{ϕ} and the source term, S_{ϕ} are defined in Table 1 for each conservation equation. The left hand side of general equation contains convection term, while the right hand side contains the diffusion and source terms.

Table 1. Conservation equations variables

Equation	ϕ	Γ_{ϕ}	S_{ϕ}
Continuity	1	0	0
Momentum x	u^{+}	1	$-\frac{dP^{+}}{dx^{+}}+\frac{w^{+2}}{r^{+}}$
Momentum y	v^{+}	1	$-\frac{dP^{+}}{dy^{+}}$
Momentum z	w^{+}	1	$-\frac{dP^{+}}{dz^{+}}$
Energy	T^{+}	1/Pr	$-w^{+}\frac{dT^{+}}{dz^{+}}$

The numerical solution procedure used in this study is based on the SIMPLE algorithm given by Patankar (1980). The equations are approximated with finite difference equations by the control volume-based finite difference method for the dependent variables, u^{+}, v^{+}, w^{+} and T^{+}. The convection and diffusion terms are discretized by using the upwind scheme and the central difference scheme, respectively. The finite difference equations for the dependent variable of interest are solved by ADI (Alternating-Direction Implicit) method (Roache, 1982). This method uses the Tri-Diagonal Matrix Algorithm, TDMA, making successive sweeps over the computational field. Because the pressure-correction equation is a Poisson equation, Alternating-Direction Implicit solution of the difference equations is replaced by the Stone's solution method (Stone, 1968). For given values of dimensionless radius of curvature, r^{+}, the dimensionless axial pressure gradient, dP^{+}/dz^{+}, the dimensionless axial temperature gradient, dT^{+}/dz^{+} and the Prandtl number, Pr, the distributions of dimensionless velocity components, u^{+}, v^{+}, w^{+}, the dimensionless distributions of temperature, T^{+}, and pressure, P^{+}, are initially guessed at each nodal location. Momentum equations for u^{+} and v^{+} are then solved to get new velocity fields for u^{+} and v^{+}. Generally, these transverse velocity fields with the initial guessed pressure field can not satisfy the continuity equation. Thus, the pressure correction equation is solved and then u^{+} and v^{+} and P^{+} are corrected accordingly. Then, u^{+} and v^{+} are updated and momentum equation for w^{+} is solved based on the corrected transversal velocity and pressure fields. A staggered grid system which is the components of u^{+} and v^{+} are defined on the control volume surfaces located at the midpoint between the main nodal grid points and all other components of w^{+}, T^{+} and P^{+} are defined at the main grid points is employed. Considering both computational cost and convergence the relaxation factor is taken as 0.5, 0.5, 1, 0.7 and 0.45 for u^{+}, v^{+}, w^{+}, T^{+} and P^{+}, respectively. To check the validity of the numerical results, grid study is performed and a uniform grid system of 100 x 100 is chosen for all the cases in this study. The solutions were assumed to converge when the following convergence criteria was satisfied for every variable at every point in the solution domain

$$\left|\frac{\phi_{new}-\phi_{old}}{\phi_{new}}\right|\le 10^{-4} \tag{16}$$

where ϕ represents u^{+}, v^{+}, w^{+} and T^{+}.

The average dimensionless axial velocity is calculated as:

$$w_{m}^{+}=\frac{\iint w^{+}dx^{+}dy^{+}}{\iint dx^{+}dy^{+}} \tag{17}$$

The Reynolds number is given as:

$$\mathrm{Re}=\frac{w_{m}D_{h}}{\nu}=w_{m}^{+} \tag{18}$$

The Dean number is defined as:

$$De=\frac{\mathrm{Re}}{\sqrt{r^{+}}} \tag{19}$$

The local Nusselt numbers can be obtained from gradients of temperatures at the channel walls with the following relationships:

$$Nu_{L}=\begin{cases}-\dfrac{\partial T^{+}}{\partial y^{+}} & for\ horizontal-walls\\ -\dfrac{\partial T^{+}}{\partial x^{+}} & for\ vertical-walls\end{cases} \tag{20}$$

The average Nusselt number on the channel and core walls can be expressed as:

$$Nu = \frac{\int_{1-2-3-4-1} Nu_L \, dl}{\int_{1-2-3-4-1} dl} \tag{21}$$

$$Nu = \frac{\int_{1'-2'-3'-4'-1'} Nu_L \, dl'}{\int_{1'-2'-3'-4'-1'} dl'} \tag{22}$$

The friction factor is given by

$$f\,\mathrm{Re} = -2\frac{dP^+ / dz^+}{w_m^+} \tag{23}$$

RESULTS AND DISCUSSION

In order to validate the present study, the results obtained are compared with the literature. The comparisons of the Dean number and friction factor ratio results obtained by Gyves (1997), Dong and Ebadian (1991), Cheng et al. (1976) and Komiyama et al. (1984) are given in Table 2 depending on the dimensionless axial pressure gradient. As can be seen in Table 2, there is very close agreement with the data available in the literature for Dean number and friction factor. Also, it seems that the Nusselt number is close agreement with the previous study by Hwang and Chao (1991) (Table 3).

Table 2. Comparison of numerical results in the curved square channel for Dean number and friction factor ratio.

dP^+/dz^+	r^+	grid	Dean number					Friction factor ratio (fRe_c / fRe_s)				
			Present Study	T.W Gyves (1997)	Cheng et al. (1976)	Komiyama et al. (1984)	Dong and Ebadian (1991)	Present Study	T.W Gyves (1997)	Cheng et al. (1976)	Komiyama et al. (1984)	Dong and Ebadian (1991)
-3900	100	30×30	14.0	14.0	13.9	14.0	14.1	1.01	1.01	1.01	1.00	1.00
		100x100	13.9	----	----	----	----	1.00	----	----	----	----
-9000	100	30×30	29.7	29.7	29.5	29.8	----	1.08	1.07	1.07	1.06	----
		100x100	30.0	----	----	----	----	1.07	----	----	----	----
-19000	100	30×30	55.0	55.2	54.8	55.4	----	1.23	1.21	1.22	1.20	----
		100x100	55.5	----	----	----	----	1.20	----	----	----	----
-39500	100	30×30	99.1	100.6	100.0	101.8	99.1	1.42	1.38	1.41	1.38	1.42
		100x100	100.8	----	----	----	----	1.40	----	----	----	----
-70000	100	40×40	151.3	151.1	151.1	150.5	----	1.65	1.63	1.63	1.63	----
		100x100	151.6	----	----	----	----	1.61	----	----	----	----
-110000	100	40×40	214.6	210.9	202.6	209.5	201.4	1.83	1.83	1.91	1.91	1.92
		100x100	215.2	----	----	----	----	1.90	----	----	----	----

Table 3. Comparison of numerical results in the curved square channel for Nusselt number ratio

Dean number		Nu_c/Nu_s	
Present study	Hwang and Chao (1991)	Present study	Hwang and Chao (1991)
0	0	1.00	1.00
101.3	100	2.06	2.00
214.6	223.6	2.79	2.95

Flow and Isotherm Patterns

The axial velocity contours are shown in Figs. 2 and 3 in the eccentric curved annular square channel for the Case A and Case B, respectively. The annulus dimension ratio (a/b) is 5.5 and the grid is 100×100. It is seen that the maximum axial velocity occurs at the middle of line connecting the lower right corners and lower left corners of the channel and the core for Case A and Case B, respectively, at the lowest Dean number (De=5.8) (Fig. 2a and 3a). It is observed that the maximum point of the axial velocity moves toward right-hand concave wall of the duct because of the centrifugal force generated by the curvature when the Dean number increases. Also, it is found that the maximum value of the axial velocity increases in the cross-section of the eccentric curved annular square duct as the Dean number increases. The rate of increase is higher in Case A than Case B. It is seen that when the Dean number increases, the axial velocity contours in the Case B differ from Case A. It is known that the effect of secondary flows increases at the region between the vertical symmetry line and right-hand concave wall of the duct because of the centrifugal force as the Dean number increases. So, it is considered that as the core is located in this region in Case B, the effect of the secondary flow is limited.

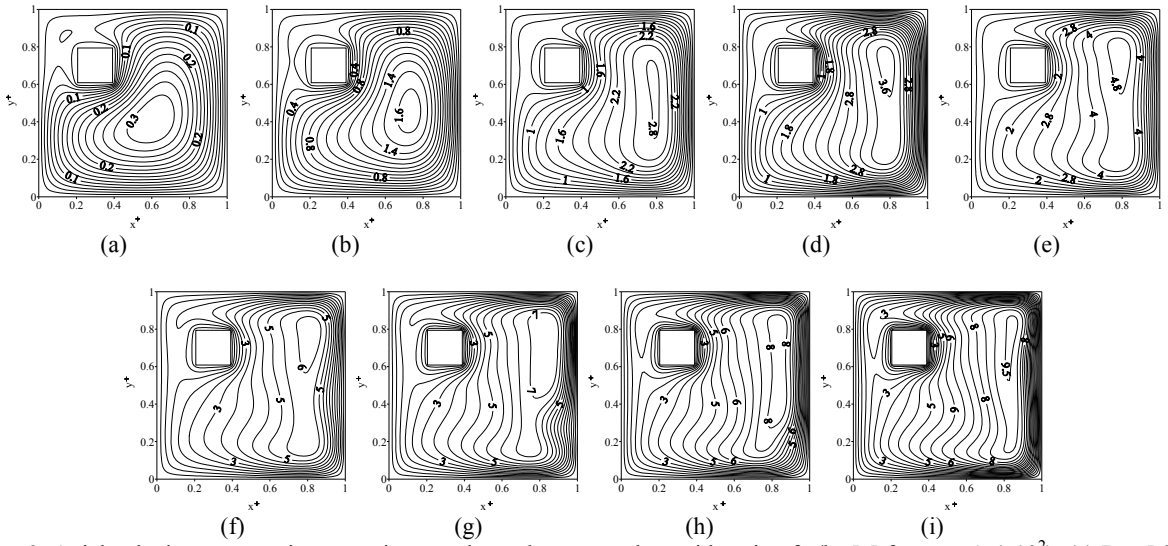

Figure 2. Axial velocity contours in eccentric curved annular square duct with ratio of a/b=5.5 for case A (x10^2): (a) De=5.8; (b) De=30.2**;** (c) De=56.9**;** (d) De=75.3**;** (e) De=102.9**;** (f) De=129.3**;** (g) De=156.6**;** (h) De=175.9**;** (i) De=207.1

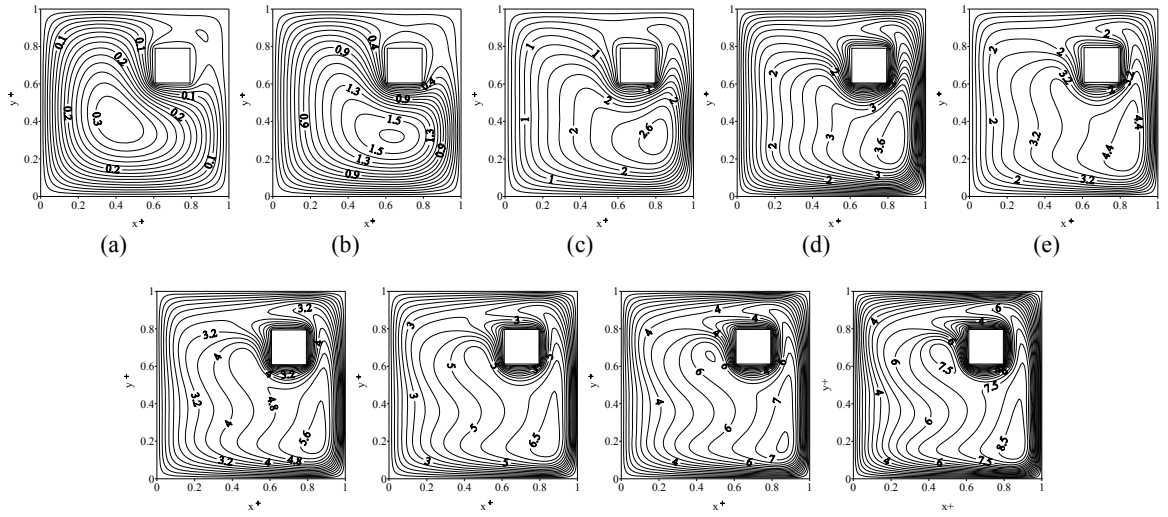

Figure 3. Axial velocity contours in eccentric curved annular square duct with ratio of a/b=5.5 for case B (x10^2): (a) De=5.8**;** (b) De=29.9**;** (c) De=51.5**;** (d) De=76.6**;** (e) De=100.8**;** (f) De=129.1**;** (g) De=156.5**;** (h) De=175.9**;** (i) De=207.2

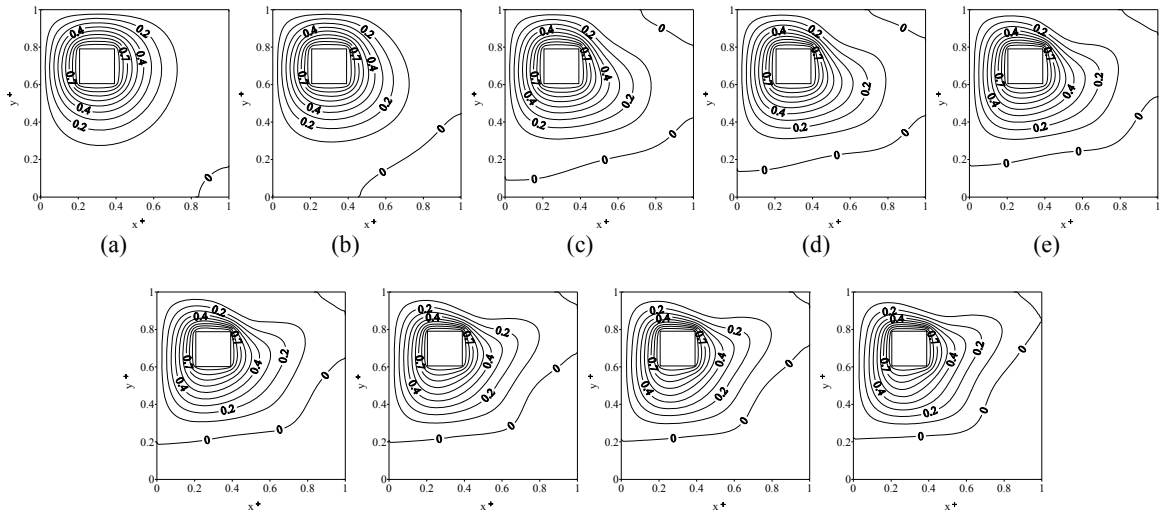

Figure 4. Temperature contours in eccentric curved annular square duct with ratio of a/b=5.5 for case A (Pr=0.7): (a) De=5.8; (b) De=30.2; (c) De=56.9; (d) De=75.3; (e) De=102.9; (f) De=129.3; (g) De=156.6; (h) De=175.9; (i) De=207.1

The temperature contours are shown in Figs. 4 and 5 for eccentric curved annular square channel with a/b=5.5 for Case A and Case B, respectively. Constant wall temperature boundary conditions are imposed at the duct and core walls. The temperature of the duct walls and the fluid is 300 K and the temperature of the core walls is 350 K. It is observed that the temperature gradient is high on the left and the upper side and right and upper side gap of the core for case A and Case B, respectively. It is found that the temperature contours are symmetrical and similar for Case A and Case B until De=30. After De=30, the temperatures contours become different from each others depending on velocity fields. It is seen that the hot fluid particles move towards left-hand convex wall and the temperature contours become parallel in the upper region of horizontal symmetry line of the channel as the Dean number increases in Case B.

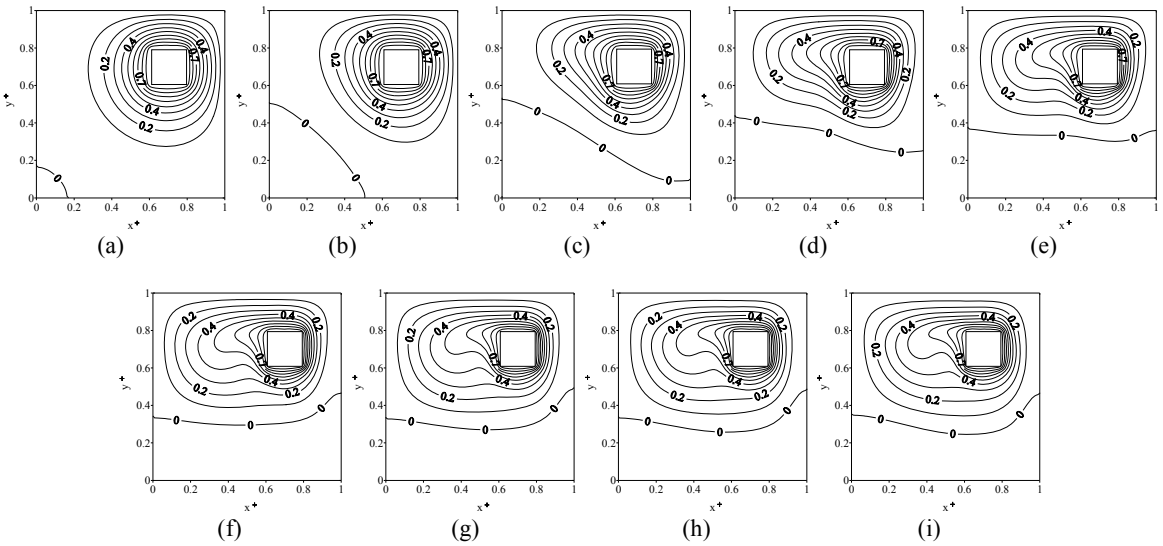

Figure 5. Temperature contours in eccentric curved annular square duct with ratio of a/b=5.5 for case B (Pr=0.7): (a) De=5.8; (b) De=29.9; (c) De=51.5; (d) De=76.6; (e) De=100.8; (f) De=129.1; (g) De=156.5; (h) De=175.9; (i) De=207.2

The secondary flow streamlines are given in Figs. 6 and 7 for Case A and Case B, respectively. The laminar flow in the eccentric curved annular channel is characterized by a secondary flow created by centrifugal force in the cross-section of the duct. The nature of this phenomenon depends on the Dean number which represents the ratio of the centrifugal force to the viscous force. While the fluid flows inside the channel, it is affected by centrifugal force generated by the curvature; therefore, the fluid particles on the center of the channel cross-section move towards right-hand concave wall of the duct. Due to the high pressure force occurring near the outer wall of the channel, the fluid particles in this section are peripherally enforced to move towards upper and lower duct walls. Since the streamwise velocity near the upper and lower wall of the channel is much smaller than that in the gap region because of the no-slip condition, the slower moving fluid particles near the upper and lower wall region have to move towards left hand convex wall to maintain the momentum balance between the centrifugal force and the pressure force. Therefore, it is seen that two main vortices occur in the duct cross-section. It is observed that one of them occurs on the upper region of the channel cross-section and it rotates in the counter-clockwise direction and also surrounds peripherally to the core for Case A and Case B. In spite of this, it is realized that the other main vortex arises on the lower region of the duct cross-section and it rotates in the clockwise direction for both Case A and Case B. It is seen that the form of the secondary flow streamlines obtained in the Case A and Case B is similar to each other at the lowest Dean number (De=5.8) (Figs. 7a and 6a). For high Dean number, it is realized that the secondary flows in Case A is more effective than Case B on the lower region of the duct. Contrary, the secondary flows in Case B is more effective than Case A on the upper region of the channel. It is determined that the main vortex settling on the lower region of the channel cross-section extends from the lower side to the upper side of the right-hand concave wall of the duct and the main vortex locating on the upper region is pushed toward the center of duct when De>129.3 in Case A. So, it can be said that the core position is remarkably important in curved annular ducts. It is observed that an additional vortex occur inside of the main vortex locating on the upper region of the duct cross-section for each case (Case A and Case B). It seems that this vortex rotates in the same direction with the main vortex and its form changes with increasing Dean number. As a result, it is found that the centrifugal and pressure forces and the core position are highly effective in the eccentric curved annular square ducts.

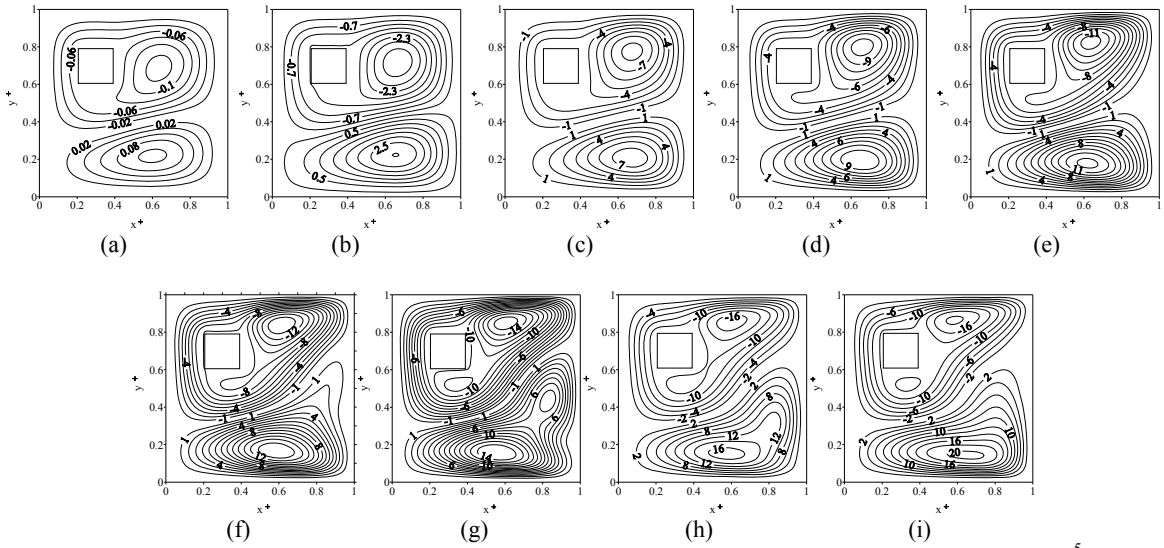

Figure 6. Secondary flow streamlines in eccentric curved annular square duct with ratio of a/b=5.5 for case A ($x10^{-5}$): (a) De=5.8; (b) De=30.2; (c) De=56.9; (d) De=75.3; (e) De=102.9; (f) De=129.3; (g) De=156.6; (h) De=175.9; (i) De=207.1

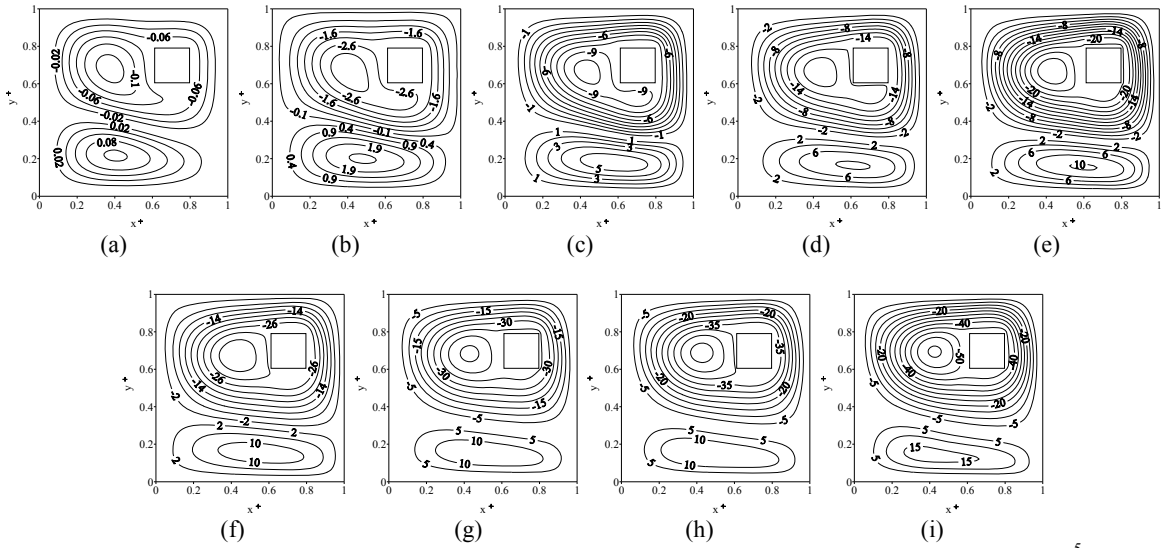

Figure 7. Secondary flow streamlines in eccentric curved annular square duct with ratio of a/b=5.5 for case B ($x10^{-5}$): (a) De=5.8; (b) De=29.9; (c) De=51.5; (d) De=76.6; (e) De=100.8; (f) De=129.1; (g) De=156.5; (h) De=175.9; (i) De=207.

The variations of the dimensionless axial velocity (w/w_m) with the Dean number are demonstrated in Figs. 8a and b for Case A and Case B with a/b=5.5 at y^+=0.5 horizontal symmetry line, respectively. It seems that when the Dean number increases the maximum value of w/w_m decreases and shifts toward right-hand concave wall of the channel because of centrifugal force. It is realized that these variations occurring in the dimensionless axial velocity are formed by the secondary flow getting in the channel cross-section and the core position.

The variations of dimensionless axial velocity (w/w_m) with the Dean number are represented in Figs. 9a and b for Case A and Case B at x^+=0.5 vertical symmetry line of the channel, respectively. It seems that the maximum value of w/w_m decreases as the Dean number increases for both Case A and Case B. Also, it is found out that two different maximum point which one of them locates near the lower wall of the channel and the other settles near the upper wall of the duct occur in the duct cross-section after De=102.9 in Case A. It is concluded that the flow field affected by the curvature and the core position highly affect the variation of dimensionless axial velocity at vertical symmetry line of the duct.

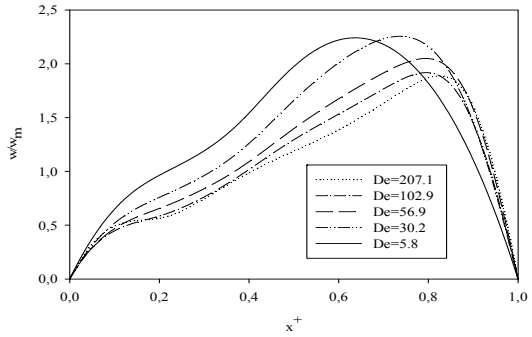

(a)

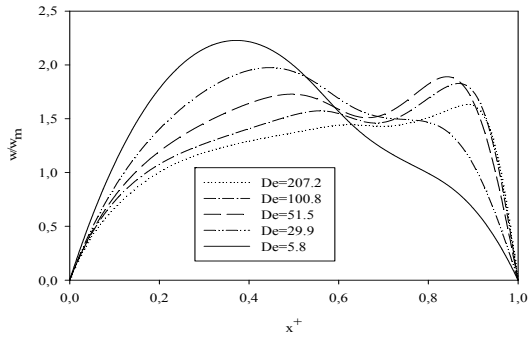

(b)

Figure 8. The effect of Dean number on dimensionless axial velocity distribution at y^+=0.5 in eccentric curved annular square duct for a/b=5.5: (a) case A; (b) case B

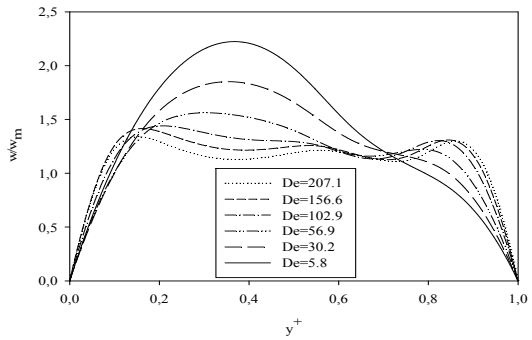

(a)

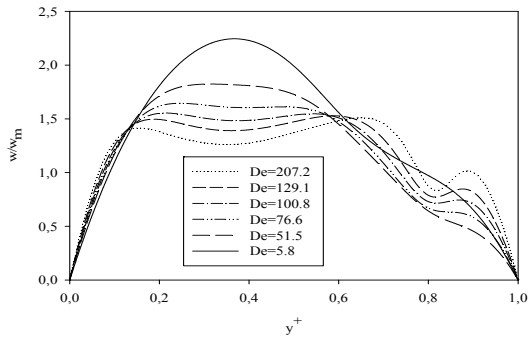

(b)

Figure 9. The effect of Dean number on dimensionless axial velocity distribution at x^+=0.5 in eccentric curved annular square duct for a/b=5.5: (a) case A; (b) case B

Nusselt Number and Friction Factor

The variations of the local Nusselt numbers computed peripherally with Eq. (20) on the duct walls for Case A and Case B with a/b=5.5 are shown in Figs. 10a and b, respectively. It is observed that the local Nusselt numbers are very low on the right-hand concave and lower walls of the duct in Case A and left hand convex and lower walls of the duct in Case B because of very low temperature gradient (see Figs. 4 and 5). However, the local Nusselt numbers are high on the left hand convex and upper walls of the channel in Case A and right hand and upper walls of the channel in Case B because of high temperature gradient (see Figs. 4 and 5). It is seen that the local Nusselt numbers decrease on the upper wall of the channel and their maximum point moves toward left-hand convex wall of the duct when the Dean number increases for Case A. It seems that the maximum value of local Nusselt number decreases and the maximum point moves toward upper wall of the duct as Dean number increases for Case B. It seems that the local Nusselt numbers increase up to De=102.9 and decrease at De=207.1 on the right-hand concave wall of the duct for Case A. Also, the local Nusselt number increases at De=51.5 and then it decreases as the Dean number increases on the upper wall for Case B. It seems that the local Nusselt numbers increase until De=129.1 and then decrease on the left-hand convex wall of the channel (Fig. 10b). As a result, it is determined that the higher local Nusselt number occurs, the higher temperature gradient take places on the channel walls. Consequently, it is realized that the local Nusselt numbers change depending on the temperature field formed by the velocity field and affected by the secondary flows.

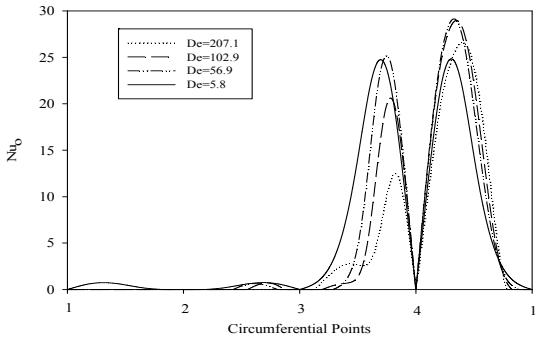

(a)

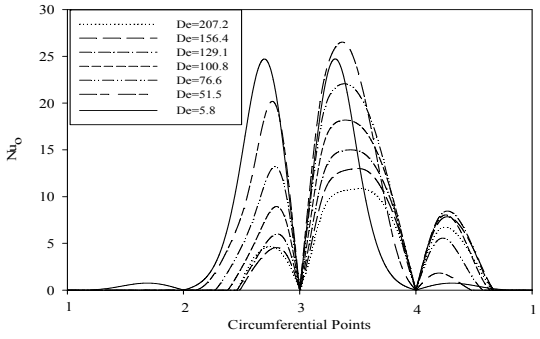

(b)

Figure 10. The variation of local Nusselt number with Dean at the channel wall of eccentric curved annular square duct for a/b=5.5 and Pr=0.7: (a) case A; (b) case B

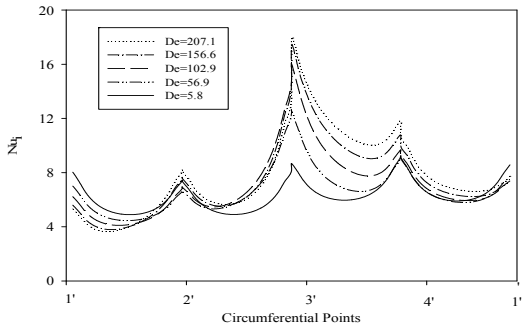

(a)

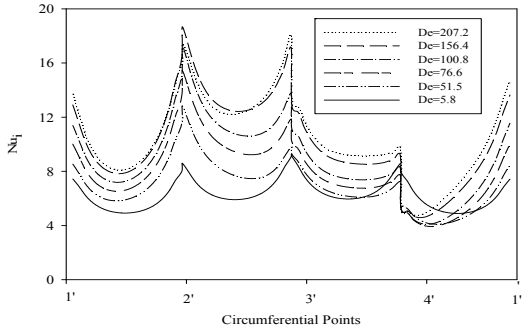

(b)

Figure 11. The variation of local Nusselt number with Dean at the core wall of eccentric curved annular square duct for a/b=5.5 and Pr=0.7: (a) case A; (b) case B

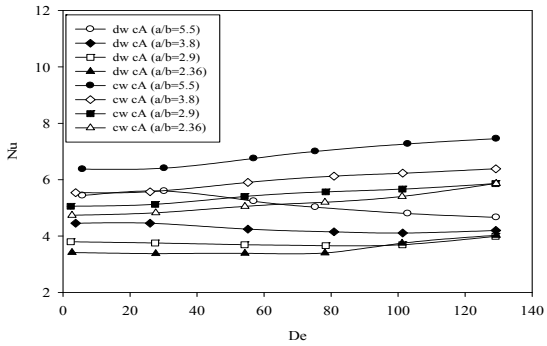

(a)

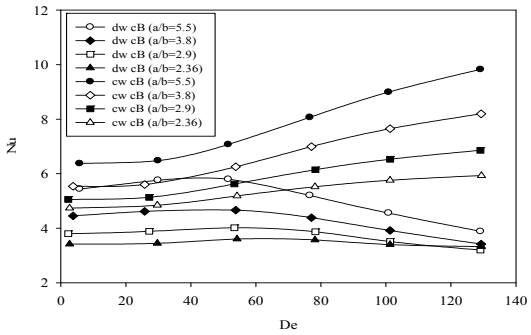

(b)

Figure 12. The variation of average Nusselt number with Dean number at core and channel wall of eccentric curved annular square duct for Pr=0.7: (a) case A; (b) case B

The variations of the local Nusselt numbers calculated peripherally with Eq. (20) on the core walls for Case A and Case B with a/b=5.5 are presented in Figs. 11a and b, respectively. It is pointed out that the local Nusselt numbers have the maximum values on the corners of the core and decrease toward middle points of the core walls. The local Nusselt numbers obtained on the upper and left-hand walls are higher than that obtained on the lower and right-hand walls of the core in Case A because the high temperature gradient (see Fig. 4). However, the local Nusselt numbers occurring on the upper and right-hand walls are higher than that occurring on the lower and left-hand walls of the core in Case B because the low temperature gradient (see Fig. 5). It is observed that on the lower wall of the core the local Nusselt numbers decrease (Fig. 11a) when the Dean number increases. It is found that the local Nusselt numbers increase on the right, left and upper walls of the core as the Dean number increases; however, the highest increasing occurs on the upper wall of the core in case A. (Fig. 11a). It is observed that the local Nusselt number increases when the Dean number increases on the all walls of the core in case B (Fig. 11b) but the highest local Nusselt number is obtained on the right wall of the core. It seems that the local Nusselt numbers increase on the upper region and decrease on the lower region of the middle point of the left core wall when the Dean number increases and minimum value of the local Nusselt number occurs on this region (Fig. 11b). As a result, it is concluded that the temperature gradient depending on temperature field directly affects the local Nusselt number. Also, it is point out that the velocity field and secondary flows also affect the local Nusselt number.

The variations of the average Nusselt number computed by using Eqs.(21-22) on the walls of duct and core with the Dean number are shown in Figs. 12a and b for Case A and Case B, respectively. It is determined that for each annulus dimension ratio (a/b), the average Nusselt number increases when the Dean number increases on the core walls. Also, it is determined that the value of the average Nusselt number decreases when the annulus dimension ratio decreases on the core wall for each case. The rate of increase on the Nusselt number with Dean number on the core walls is higher in Case B than those in Case A. This results from the fact that the maximum velocity of the fluid moves towards right-hand concave wall of the channel when Dean number increases (the core is placed into this maximum velocity field in Case B). So, the temperature gradient is higher in case B than that in Case A. It is found that the value of the average Nusselt number decreases when the annulus dimension ratio decreases on the channel wall. It seems that different variations occur in the average Nusselt number with Dean number for each case depending on the temperature field affected by velocity field on the channel wall. Because of breaking down of maximum flow field by the core, decreasing of Nusselt number with Dean number in case B is higher than those in Case A on the channel wall.

The variations of the friction factor (fRe) with the Dean number are presented in Figs. 13a and b for the Case A and Case B, respectively. It is determined that the value of fRe increases when the Dean number increases. Besides this, it is seen that the value fRe increases when the values of the annulus dimension ratio decrease. In

Case B, as the core is placed near the right-hand concave wall- the maximum velocities move towards this region with increasing of Dean number- the flow field is broken down and the friction factor increases. For this reason as seen in Figs. 13 a and b, the friction factor (fRe) is higher in Case B than Case A by increasing of Dean number. It seems that at the high Dean number, the differences between values of fRe resulting from the ratio of a/b decrease and their values approach each other. After De>60, the effects of centrifugal and pressure forces on the flow field and heat transfer are more dominant than viscous forces. The effects of centrifugal and pressure forces on the flow field for De<60 is limited and for all a/b ratios this effect is almost the same.

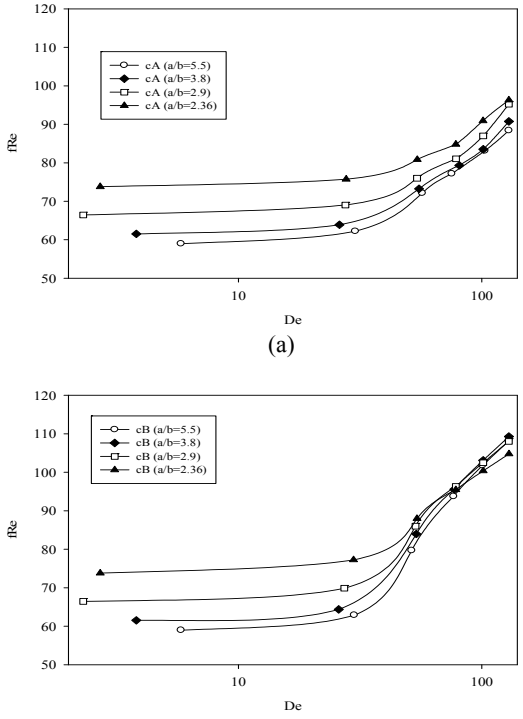

Figure 13. The variation of friction factor with Dean number in eccentric curved annular square duct: (a) case A; (b) case B

CONCLUSION

Hydrodynamically and thermally fully developed, steady, incompressible laminar flow with constant physical properties in eccentric curved annular duct is numerically investigated under constant wall temperature boundary condition peripherally. Solutions are obtained for Dean number ranges from 2.8 to 207.2, Prandtl number 0.7.

The laminar flow in the eccentric curved annular channel is characterized by a secondary flow created by centrifugal force in the cross-section of the duct for both Case A and Case B. The secondary flow resulting from centrifugal force highly affects the velocity and temperature fields. Because of the centrifugal force generated by the curvature, the maximum point of the axial velocity moves toward right-hand concave wall of the duct when the Dean number increases. The value of maximum velocity is higher in Case A than Case B because of the location of the core as Dean number increases. The curvature, annulus dimension ratio and core position affect heat transfer and friction factor. When the annulus dimension ratio increase the convective heat transfer is remarkably enhanced at both the inner and the outer walls.

The temperature gradient depending on temperature and fields and secondary flows directly affects the local and average Nusselt number. The rate of increase on the Nusselt number with Dean number is higher in Case B than those in Case A on the core wall. However, the rate of decrease on the Nusselt number with Dean number is higher in case B than those in Case A on the channel wall. The average Nusselt number increases on both core and channel walls when the annulus dimension ratio increases for each case. The average Nusselt number is higher on the core wall than duct wall for each annulus dimension ratio. The average Nusselt number increases on the core walls as the Dean number increases.

The friction factor (fRe) is higher in Case B than Case A by increasing of Dean number. After De>60, the effects of centrifugal and pressure forces on the flow field and heat transfer are more dominant than viscous forces. The effects of centrifugal and pressure forces on the flow field for De<60 is limited and for all a/b ratios this effect is almost the same. When the eccentric curved annular ducts are compared with each other the highest friction loses become in the ducts with lower annulus dimension ratio.

REFERENCES

Asan, H. and Kucuk, H., A Numerical Computation of Heat and Fluid Flow in L-Shaped Curved Channels, *Heat Transfer Engineering* 28, 112-119, 2007.

Cheng, K. C., Lin, R-C. and Ou, J-W., Fully Developed Laminar Flow in Curved Rectangular Channels, *Journal of Fluid Engineering* 98, 41-48, 1976.

Choi, H. K. and Park, S. O., Laminar Entrance Flow in Curved Annular Ducts, *Int. J. Heat and Fluid Flow* 13, 41-49, 1992.

Choi, H. K. and Park, S. O., Mixed Convection Flow in Curved Annular Ducts, *Int. J. Heat Mass Transfer* 37, 2761-2769, 1994.

Çengel, Y. A., *Heat Transfer: A Practical Approach* (Second Ed.), McGraw-Hill, New York, 2003

Dong, Z. F. and Ebadian, M. A., Numerical Analysis of Laminar Flow in Curved Elliptic Ducts, *J. Fluids Engineering* 113, 555-562, 1991.

Dong, Z. F. and Ebadian, M. A., Effects of Buoyancy on Laminar Flow in Curved Elliptic Ducts, *Journal of Heat Transfer* 114, 936-943, 1992.

Garimella, S., Richards, D. E. and Christensen, R. N., Experimental Investigation of Heat Transfer in Coiled Annular Ducts, *Journal of Heat Transfer* 110, 329-336, 1988.

Gyves, T. W., *A Numerical Solution to Conjugated Mixed Convection Heat Transfer in Curved Square Channel*, PhD Thesis, State University of New York at Stony Brook USA, 1997.

Gyves, T. W. and Irvine, T. F., Laminar Conjugated Forced Convection Heat Transfer in Curved Rectangular Channels, *Int. J. Heat and Mass Transfer* 43, 3953-3964, 2000.

Gyves, T. W., Irvine, T. F. and Naraghi, M. H. N., Gravitational and Centrifugal Buoyancy Effects in Curved Square Channels with Conjugated Boundary Conditions, *Int. J. Heat and Mass Transfer* 42, 2015-2029, 1999.

Hwang, G. J. and Chao, C-H., Forced Laminar Convection in a Curved Isothermal Square Duct, *Journal of Heat Transfer* 113, 48-55, 1991.

Incropera, F. P. and DeWitt, D. P. *Fundamentals of Heat and Mass Transfer* (Third Ed.), Wiley, Singapore, 1990.

Komiyama, Y., Mikami, F., Okui, K. and Hori, T., Laminar Forced Convection Heat Transfer in Curved Rectangular Cross-section, *Heat Transfer Japanese Research*, 22, 68-91, 1984.

Kucuk, H., *Numerical Investigation of Heat Transfer and Fluid Flow in Concentric or Eccentric Curved Annular Ducts* PhD Thesis, Karadeniz Technical University, Trabzon, Turkey, 2003.

Kucuk, H. and Asan, H, A Numerical Study on Heat and Fluid Flow in Concentric Curved Annular Square Ducts, *Heat Transfer Engineering* 30 (5), 383-392, 2009

Patankar, S.V. *Numerical Heat Transfer and Fluid Flow,* Hemisphere, Washington, DC, 1980.

Petrakis, M. A. and Karahalios, G. T., Exponentially Decaying Flow in a Gently Curved Annular Pipe, *Int. J. Non-Linear Mechanics* 32, 823-835, 1997.

Petrakis, M. A. and Karahalios, G. T., Fluid Flow Behaviour in a Curved Annular Conduit, *Int. J. Non-Linear Mechanics* 34, 13-25, 1999.

Roache, P. J., *Computational Fluid Dynamics* (fifth Ed.), Hermosa Publishers, Albuquerque, New Mexico, 1982.

Stone, H. L. Iterative Solution of Implicit Approximations of Multi-dimensional Partial Differential Equations, *SIAM J. Numer. Anal.* 5, 530-558, 1968.

Haydar Kucuk is an assistant professor at Karadeniz Technical University, Trabzon, Turkey. He received his Ph.D. in 2003 from Karadeniz Technical University. His research interests involve numerical heat transfer and fluid flow, drying and drying models, energy and exergy analyses. He has published 16 articles in recognized journals and proceedings.

Habip Asan is a professor at Karadeniz Technical University, Trabzon, Turkey. He received his Ph.D. in 1993 from Texas Tech University, Lubbock, Texas, USA. His main research interests are CFD, numerical heat transfer, heat transfer enhancement and optimum thermal insulation of buildings. He has published more than 25 articles in recognized journals and proceedings.